Applied Energy 343 (2023) 121194

Contents lists available at ScienceDirect

Applied Energy

journal homepage: www.elsevier.com/locate/apenergy

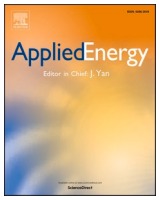

Experimental investigation of a reverse osmosis desalination system directly powered by wave energy

Jia Mi [a,b], Xian Wu [a,b], Joseph Capper [b], Xiaofan Li [a,b], Ahmed Shalaby [c], Ruoyu Wang [d], Shihong Lin [d], Muhammad Hajj [c], Lei Zuo [a,b,*]

[a] Department of Naval Architecture and Marine Engineering, University of Michigan, Ann Arbor, MI 48109, USA
[b] Department of Mechanical Engineering, Virginia Tech, Blacksburg, VA 24061, USA
[c] Department of Civil, Environmental and Ocean Engineering, Stevens Institute of Technology, Hoboken, NJ 07030, USA
[d] Department of Civil and Environmental Engineering, Vanderbilt University, Nashville, TN 37212, USA

HIGHLIGHTS

- A novel ocean wave powered reverse osmosis desalination system is introduced.
- An integrated system demonstration in wave tank is presented and investigated.
- The role of key component tuning on system performance is experimentally quantified.
- Specific water productivity is determined and analyzed in different sea states.
- Performance in a real application scenario is predicted via pilot demonstration.

GRAPHICAL ABSTRACT

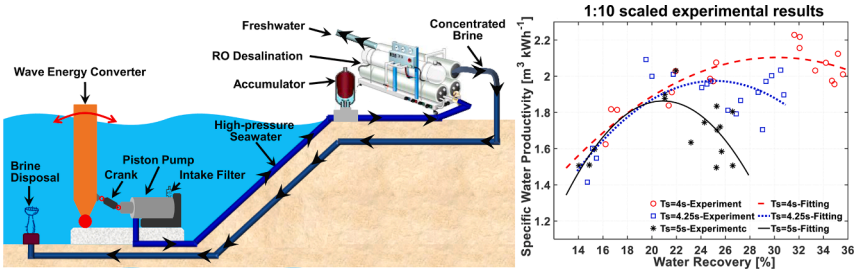

ARTICLE INFO

Keywords:
Desalination
Wave energy converter
Reverse osmosis
Pilot study
Wave tank test

ABSTRACT

Powering desalination processes with renewable energy is a promising solution to address the global issue of water shortage with minimum carbon footprint and environmental impact. We experimentally investigate a sustainable reverse osmosis (RO) desalination system directly powered by wave energy. In this system, seawater is pressurized and pumped to a RO desalination module via a piston pump directly driven by an oscillating surge wave energy converter (OSWEC). An accumulator is adopted on the feed inlet to mitigate the pressure fluctuations under time-varying ocean conditions. Meanwhile, a needle valve on the brine outlet is used to adjust the system pressure and water recovery. A 1:10 scaled model was designed, fabricated, and tested in a wave tank based on the Froude scaling law. The optimal specific water productivity (SWP) obtained in the tank tests with 3.5 g/L feed salinity was 2.23 m^3/kWh, indicating a full-scale specific water productivity of 0.22 m^3/kWh for 35 g/L seawater salinity. The influence of needle valve tuning on the specific water productivity was experimentally investigated and analyzed. Under a specific operational condition, tuning this valve improved specific water productivity by about 17 % and reduced the system pressure by 24 %, thereby avoiding extreme pressure and improving the system's capability. This pilot study demonstrates that ocean wave energy is a promising source to sustainably power reverse osmosis desalination and provide freshwater water for coastal regions.

* Corresponding author at: Department of Naval Architecture and Marine Engineering, University of Michigan, Ann Arbor, 48109, USA.
E-mail address: leizuo@umich.edu (L. Zuo).

https://doi.org/10.1016/j.apenergy.2023.121194
Received 1 December 2022; Received in revised form 23 March 2023; Accepted 21 April 2023
Available online 12 May 2023

Nomenclature

RO	Reverse osmosis
WEC	Wave energy converter
OSWEC	Oscillating surge wave energy converter
LCOW	Levelized cost of water, $/m^3
SWP	Specific water productivity, m^3/kWh
λ	Scaling factor
i	Van's Hoff's factor
R	Ideal gas constant
T	Temperature, K
$\Delta\pi$	Osmotic pressure, Pa
c	Molar concentration, mol/L
T_s	Wave period, s
H_s	Wave height, m
P_{in}	Input power, W
F_P	Piston force, N
v_P	Piston velocity, m/s
Δp	Piston pressure, Pa
A_P	Piston area, cm^2
Q_f	Pumping flow rate, m^3/s
J_w	Permeate flux, L m^{-2}h^{-1}
J_s	Salt flux, g m^{-2}h^{-1}
A_w	Water permeability coefficient, m^3 m^{-2} s^{-1} Pa^{-1}
B_s	Salt permeability coefficient, m/s
C_m	Salt concentration in membrane side, g/L
C_p	Salt concentration in permeate, g/L

1. Introduction

Over 70 % of the earth's surface is covered in water, and 80 % of the world's population lives in coastal zones [1]. Still, over 97 % of water on earth is saline, making it unfit for drinking, irrigating crop and most industrial purposes [2]. According to the estimation by the United Nations (UN), around one kid dies from water-related issues every 9 mins, and by 2050, over than 2 billion people in around 50 countries will endure water crisis [3]. In the USA, about one million residents in California are exposed to contaminated water every year. Additionally, there will be a freshwater supply shortfall in around 40 states in the upcoming decades [4]. To address the challenge of water scarcity and achieve water security, desalination has been investigated as an alternative approach to produce fresh water. Reverse osmosis (RO), a pressure-driven separation using semipermeable membranes, has been widely used for seawater desalination due to its high energy efficiency and technical maturity [5]. Although RO-based seawater desalination is a reliable solution to the water challenges in coastal regions, nearly all desalination plants are powered by fossil fuels, which adds a carbon footprint and is thus not sustainable especially in relation to its impact on climate change [6].

Achieving sustainable seawater desalination requires the use of renewable energy. Marine renewable energy has enormous potential and ocean wave energy in the coastal regions has a high power density of around 10–20 kW/m of wave front width and can be as 100 kW/m offshore [7]. In the USA, the amount of technical available wave energy is equivalent to 34 % of the yearly electricity generation from all resources [8]. Moreover, because marine renewable energy is present where seawater is, it can be leveraged for sustainable and economic seawater desalination.

Several designs have been proposed to power RO desalination systems by using wave energy [9]. An oscillating water column (OWC) was proposed to convert ocean wave energy to electricity first, and then power RO desalination [10]. A translational pump driven by a floating buoy was proposed to directly pressurize the seawater without electricity [11]. In recent years, bottom-hinged oscillating surge wave energy converters (OSWECs) have been widely investigated for nearshore sustainable desalination because of the dominant surge motions in the nearshore region [12–14]. OSWEC was investigated to transfer seawater to the desalination plant on shore [15]. Additionally, variants of OSWECs have been investigated, such as the self-floating configuration to extend the OSWEC from nearshore region to offshore region, and a portable configuration for personal use [16,17].

Dynamic modeling of the wave powered desalination system has been presented in different studies. A transient one-dimensional model of a wave-powered RO system indicated that the such a system delivers a larger quantity of permeate per unit energy supplied than conventional RO [18]. A bottom-hinged OSWEC with a unique adaptive pressure generator was investigated and the optimum operating pressure was determined to be around 45 bars, a lower value than the traditional 60–65 bars [14]. Yu and Jenne (2018) showed that a wave energy converter (WEC) array could be a viable, near-term solution to the freshwater supply [19]. Meanwhile, simulation results of a direct-drive wave-powered desalination system indicated that the specific energy consumption (*SEC*) could be around 2–4 kWh m^{-3} in different sea states [20]. Simulation results showed an ocean wave powered desalination plant could meet the water needs of almost 1370 residential inhabitants with a large Pelamis WEC (120 m long by 3.5 m diameter) [21]. Other simulation results indicated that an accumulator could mitigate pressure fluctuations under time-varying excitation input and improve the system's performance [19,22].

Other studies considered the techno-economic aspects of ocean wave powered desalination systems. Modeling results showed that sustaining a water recovery of about 25 % might eliminate the necessity for chemical pre-treatment [13]. The levelized cost of water (LCOW) was determined to be as low as €0.45/m^3 (value in 2009) based on a techno-economic analysis of a desalination plant powered by wave energy [23]. The economic feasibility of wave powered desalination systems in the USA was investigated and the LCOW was estimated to be around $1.79/m^3 (value in 2017) with a 100-device array [24].

Wave tank testing of scaled models is an effective way to experimentally evaluate the characteristics and performance of WECs. Experimental research on two floating OWC devices were conducted in a wave tank, and mooring loads were measured during survivability testing [25,26]. A novel mechanical motion rectifier based power take-off (PTO) was applied to a WEC and evaluated via tank tests [27]. Hydrodynamics of a dual-flap floating OSWEC were experimentally evaluated via wave tank tests, and numerical modeling could accurately simulate the response for difference cases [28].Wave tank tests of an offshore floating moored WEC were discussed and compared to a fixed design with the same geometry. The experiment results found that the surge motion of the floating device improves the power extraction efficiency [29]. A three-dimensional offshore stationary WEC was experimentally evaluated via a 1:50 scaled model and the impacts of scaling and air compressibility on the system performance were investigated [30].

Although theoretical investigation in literature has revealed promising results of ocean wave powered desalination systems. Efforts devoted to experimentally investigate the performance and characteristics of integrated wave powered desalination systems have been minimal and limited in literature. A 22 kW (30 hp) motor was used to mimic the variable ocean energy input and laboratory experiments resulted in 10 L/min freshwater production with good permeate quality (total dissolved solids less than 500 ppm) [10]. More practical experimental work could be valuable is recommended in [31], after the analysis of a RO powered by ocean wave power via a variable DC source emulating the

response of a renewable energy system. All of these laboratory experiments that are based on motor driven systems to mimic the variable ocean wave energy provided encouraging results. However, the performance of a system level experiment that integrates a WEC and a RO module under wave excitation hasn't been documented well in literature. In addition, a better understanding of the role of key component tuning on the system performance under different operation conditions is important, which will help predict and optimize system's performance in real application scenarios.

In this study, we experimentally investigated the characteristics and performance of the ocean wave powered desalination system to develop insights into its capabilities, operational opportunities and challenges. A 1:10 scaled model was designed, fabricated and tested in a wave tank. Specific water productivity was analyzed using the hydraulic performance of the piston pump and the RO module outputs (i.e., concentrated brine and permeate). The influence of the needle valve tuning on the brine outlet was investigated under different scenarios and the role of the valve tuning in improving the system performance is quantified. The contributions and novelties of this study are (1) to introduce a novel system design for sustainable desalination system directly powered by wave energy; (2) to experimentally investigate the performance and characteristics of the proposed system; (3) to evaluate the role of key component tuning on the system performance under different operating conditions; and (4) to predict the practical performance and compare to different application scenarios via pilot experiments.

The rest of this paper is organized as follows. Section 2 introduces the design concept and working principle of the investigated ocean wave powered reverse osmosis desalination system. Section 3 discusses the experimental setup and modeling analysis. Section 4 summarizes and discusses the wave tank test results. Section 5 provides concluding remarks.

2. Design concept and working principle

The proposed wave powered desalination system consists of an OSWEC with a piston pump and an onshore RO desalination module with an accumulator, as schematically shown in Fig. 1. One end of the piston pump is hinged on the seabed while the other end is attached to the OSWEC. As such, the rotational motion of the OSWEC can drive the piston pump bidirectionally. Because the piston pump is driven by the OSWEC bidirectionally, a double-acting piston pump is adopted to rectify the bidirectional motion of the piston into unidirectional hydraulic flow motion. To regulate the fluctuating feed pressure on the RO membrane under time-varying wave conditions, a bladder-type accumulator is adopted on the feed inlet [19]. The bladder inside the accumulator can be pre-charged to a certain pressure with inert gas (usually Nitrogen). When the waves amplitudes are relatively large, the pump flow rate of the piston pump will increase. As such, the bladder will be further compressed to store extra pressurized seawater, and the system pressure will increase. When wave amplitudes are relatively small, the pump rate of the piston pump will decrease. The pressurized gas inside the accumulator will cause the bladder to rebound, reducing the accumulated fluid. Therefore, releasing the pressurized seawater inside the accumulator can compensate for the reduction in feed flow rate and system pressure. Because of the pre-charged accumulator on the feed inlet, the system pressure will be regulated, and the hydraulic system performance can be improved [19,32]. In addition, a needle valve on the brine outlet is used to adjust the system pressure and water recovery under different sea states.

The energy flow and water flow of the integrated system are presented in Fig. 2. As for the energy flow, hydrokinetic energy of the ocean waves is captured by the WEC to drive the piston pump as mechanical energy. The captured mechanical energy pressurizes the seawater in the form of hydraulic energy. This energy is then applied to the RO membrane to drive the crossflow filtration. As for the water flow, seawater is pressurized and the applied pressure overcomes the seawater's osmotic pressure. The water is allowed to pass to the other side as permeate (i.e., freshwater), while the solute is retained on the pressurized side of the membrane and becomes concentrated brine.

3. Experiment setup and analysis

3.1. Prototype scaling and setup

To evaluate the overall performance of the proposed concept, an integrated system was fabricated, assembled, and tested in the wave tank (95.40 m length by 4.90 m width by 1.98 m depth) at the Davidson Laboratory of Stevens Institute of Technology. A schematic of the experimental setup is shown in Fig. 3.

Given that a typical OSWEC system will have a width of about 18 m [19], and considering the capacity of the test facility, the model was scaled based on the Froude scaling law with a scaling factor of 10 (i.e., $\lambda = 10$), as shown in Table 1 [33]. Thus, the dimensions of the 1:10 scaled OSWEC in this study were 1.8 m (width) by 0.9 m (height) by 0.23 m (thickness).

Since nearly one million Californians are exposed to unsafe drinking water each year, one specific coastal area in California (*Long Beach Channel*, Latitude: 33.70 N & Longitude: −118.20 E) was selected as the

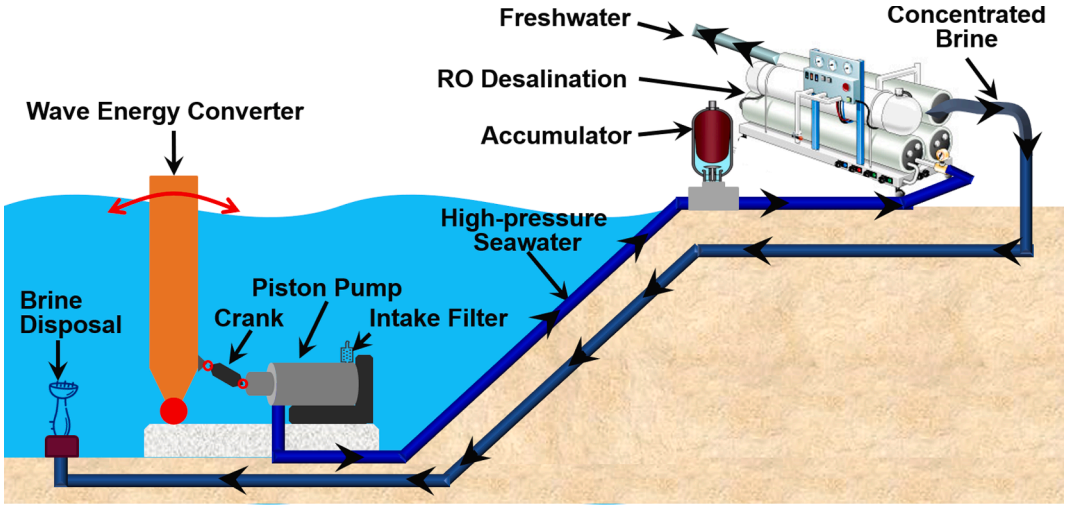

Fig. 1. Overall schematic of the proposed ocean wave powered desalination system.Seawater is pressurized by the wave energy converter and pumped to the reverse osmosis desalination module to produce freshwater.

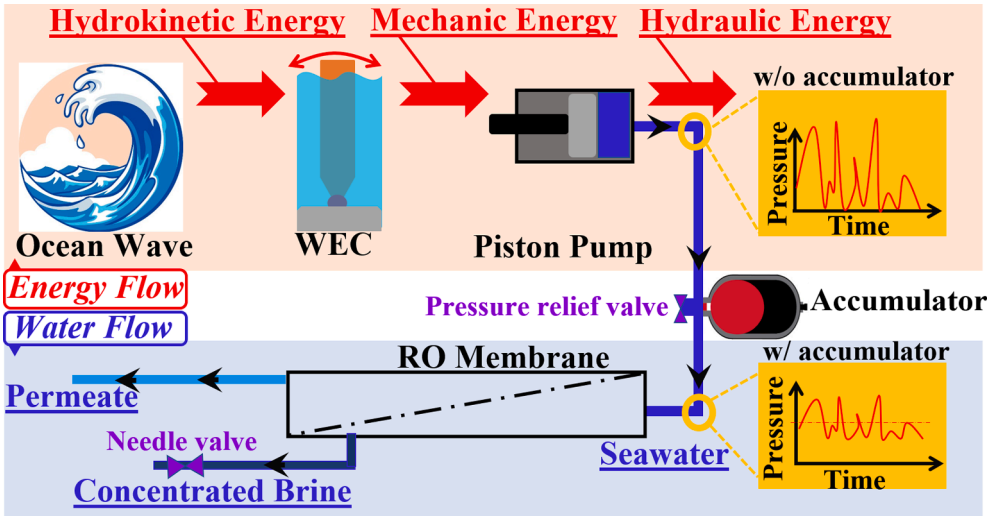

Fig. 2. Energy flow and water flow of the proposed system.

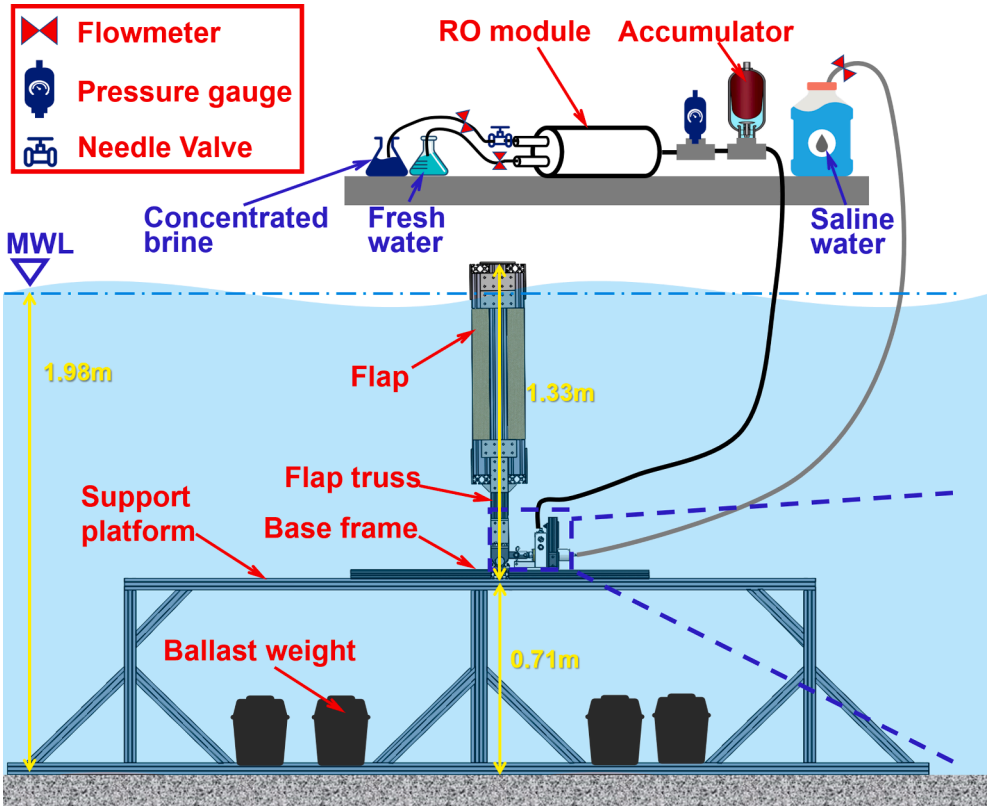

Fig. 3. Schematic of the experiment setup.

target application region [4]. The measured and recorded wave conditions in the specified location could be found in the *Coast Data Information Program* (CDIP [34]). It should be noted that wave conditions vary a lot in different locations and different seasons [35]. In this pilot study, we chose a specific location and several typical wave conditions as a target application scenario. More wave conditions considering extreme cases are worth to be investigated in the future, and wave conditions in other locations should be determined accordingly. Because the dimensions of the OSWEC and wave conditions were scaled by a factor of 10, the parameters for RO desalination were also scaled down with the same factor. The osmotic pressure of the saline water is proportional to the solution concentration, as defined in Equation (1). The concentration of seawater is typically about 35 g/L [36]. With a scaling factor of $\lambda = 10$, the scaled feed concentration was 3.50 g/L and the corresponding osmotic pressure can be calculated as

$$\Delta\pi = icRT \tag{1}$$

where $\Delta\pi$ is the osmotic pressure, i is the Van't Hoff's factor (a measure of the effects of a solute on colligative properties), c is the molar concentration of the solution, R is the ideal gas constant (8.31 J K^{-1} mol^{-1}), and T is the temperature in Kelvin (293 K, i.e., 20 °C, for ideal ambient temperature).

In the experimental setup, the OSWEC and the piston pump were submerged, while the RO desalination module was placed above the

Table 1
Froude scaling law for various quantities [33].

Quantity	Unit	Scaling
Wave height	m	λ
Wave period	s	$\lambda^{0.5}$
Length	m	λ
Mass	kg	λ^3
Density	kg m^{-3}	λ
Linear displacement	m	λ
Angular displacement	rad	1
Linear velocity	m s^{-1}	$\lambda^{0.5}$
Angular velocity	rad s^{-1}	$\lambda^{-0.5}$
Force	N	λ^3
Torque	N m	λ^4
Power	w	$\lambda^{3.5}$
Pressure	Pa	λ

λ is the geometric scale. When the scaling is 1, the quantity is not affected by scale.

water. The inlet of the piston pump was connected to the saline water reservoir and the outlet was connected to the bladder-type accumulator. The flap was hinged on the base frame with plain bearings with a crank to drive the piston pump. In such a case, the saline water was pumped from the reservoir tank via the piston pump and pressurized through the bladder-type accumulator. Then, the pressurized saline water was pushed into the RO module. As for the RO module, a spiral-wound RO membrane was mounted inside a fiber-glass housing with one inlet and two outlets. One of the outlets (connected with a needle-valve) was used to collect the concentrated brine. The other outlet was used to collect the permeate (i.e., freshwater) from the RO membrane under applied pressure. The overall system pressure and water recovery (permeate volume over input saline water volume) were controlled by adjusting the needle valve. Pictures of the fabricated model, integrated set-up and measurement connections are presented in Fig. 4.

To keep the OSWEC in the desired position in water, ballast weights were placed on the supporting platform. Based on numerical simulations, we determined that a top-piercing flap could achieve a larger power output than totally submerged ones [12]. Because the water depth in the wave tank was 1.98 m and the total height of the flap with the truss was around 1.33 m, a supporting platform with 0.71 m height was adopted. In such a case, the total height of the model was around 2.04 m, with 0.06 m of the flap's top part piercing the mean water level (MWL) in the static equilibrium position. The integrated model was assembled using mostly off-the-shelf components. A commercially available hydraulic hand pump was modified, as shown in Fig. 4c. Because the area of the rod is around half of the piston's area, the pumping rates of the two strokes (i.e., upward and downward) are the same. The mass properties and dimensions of the OSWEC are presented in Table 2.

The components of the RO desalination module were mounted on a crossing bridge 0.5 m above the water. The bladder of the accumulator was pre-charged to 3 bars with inert gas (i.e., Nitrogen), which was close to the osmotic pressure of the saline water [19]. The RO membrane used in the experiment was from the *Applied Membrane Inc* (serial number: M-

Table 2
Mass properties and dimensions of the oscillating surge wave energy converter.

Parameters	Value (unit)
Flap size	1.80 m (width) by 0.90 m (height) by 0.23 m (thickness).
Flap weight	57.60 kg
Foam density	25.63 kg m^{-3}
Flap truss height	0.43 m
Support platform height	0.71 m
Piston area	11.46 cm^2 (diameter 3.82 cm)
Rod area	5.72 cm^2 (diameter 2.70 cm)
Pump effective stroke	4.20 cm

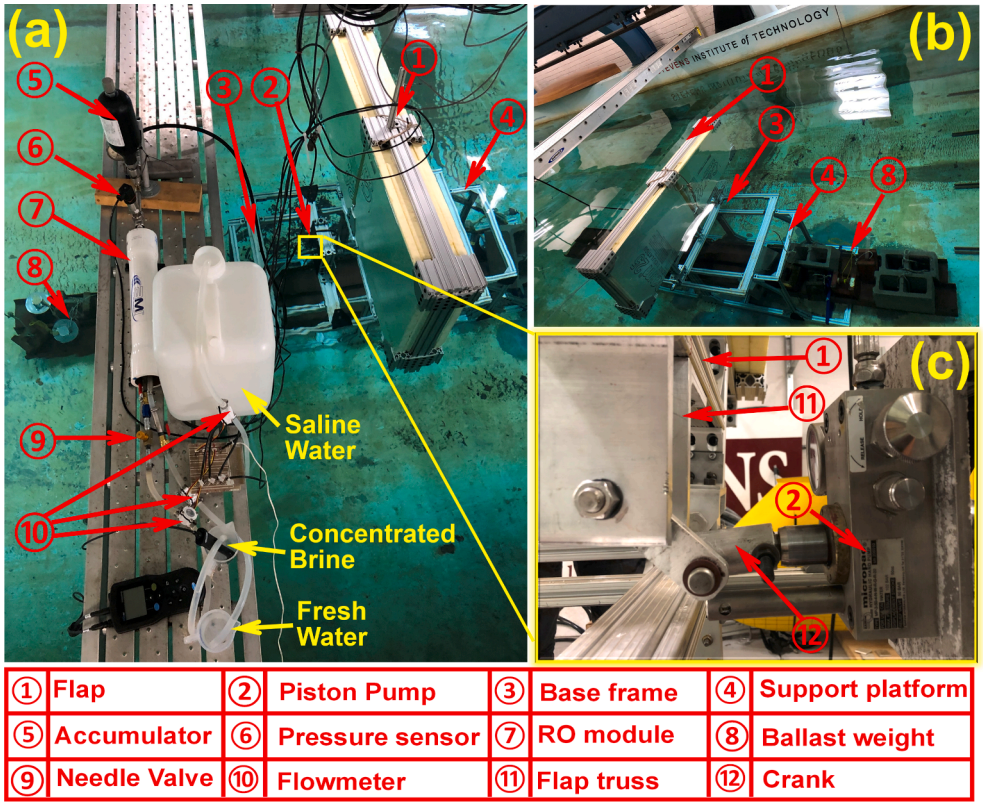

Fig. 4. Wave tank test set-up (a). Overall assembly of the oscillating surge wave energy converter; (b) Side-view of the overall deployment; (c). Enlarged view of piston pump and connections.

S2514A)), and the permeability coefficients were characterized in [37]. The RO membrane was placed inside a fiberglass pressure vessel. To prepare the saline water with the concentration of 3.5 g/L (1:10 scale), lab-grade sodium chloride (i.e., NaCl/ ACS reagent over 99.0 % from *Sigma-Aldrich*) was dissolved in purified water. Key parameters and specifications of the RO desalination module are presented in Table 3. A portable conductivity & total dissolved solids (TDS) meter (*Hach HQ14D*) was used for salt concentration measurement during the experiment. To measure the flow rate, inline turbine-type water flow sensors were used.

3.2. Modeling and analysis

To investigate the experimental results and characterize system performance, expressions for analysis are introduced. The input power P_{in} from the piston pump into the RO desalination module are calculated from the piston force F_P and velocity v_P, as described in Equation (2). The piston force F_P is obtained by multiplying the applied pressure Δp and effective piston area A_P, as described in Equation (3). The pumping flow rate Q_f from the double-acting pump is calculated based on the translational velocity of the piston pump v_P, as described in Equation (4).

$$P_{in} = F_P v_P \tag{2}$$

$$F_P = \Delta p A_P \tag{3}$$

$$Q_f = A_P v_P \tag{4}$$

As discussed in Section 2, this integrated system produces freshwater by a continuous single-pass RO module. The proposed ocean wave powered RO desalination system can continuously produce permeate over the operation phase once the hydraulic pressure provided by the piston pump exceeds the osmotic pressure of saline water. The solution-diffusion model can be used to calculate the permeate production through the RO membrane [22]. The permeate water flux J_w is proportional to the net driving pressure ($\Delta p - \Delta\pi$) while salt flux J_s is proportional to the salinity difference across the membrane ($C_m - C_p$) and are respectively expressed as

$$J_w = A_w(\Delta p - \Delta\pi) \tag{5}$$

$$J_s = B_s(C_m - C_p) \tag{6}$$

where A_w ($m^3m^{-2}s^{-1}Pa^{-1}$) is the water permeability coefficient, B_s is the salt permeability coefficient (m/s), C_m is the salt concentration on the membrane side, and C_p is the salt concentration in the permeate. If the concentration polarization is neglected, C_m can be treated as equal to the salt concentration in the bulk saline water supply [39].

The water recovery (*WR*) is defined as the ratio of permeate flux J_w and feed flux J_f, i.e.,

$$WR = \frac{J_w}{J_f} \tag{7}$$

The salt rejection (*SR*) is defined as the concentration difference between feed and permeate over feed salt concentration, i.e.,

$$SR = \frac{C_m - C_p}{C_m} \tag{8}$$

Furthermore, the permeate salt concentration C_p is related to the seawater salt concentration and net driving pressure (i.e., $\Delta p - \Delta\pi$) according to [19].

$$C_p = \frac{C_m}{\frac{A_w}{B_s}(\Delta p - \Delta\pi) + 1} \tag{9}$$

Table 3
Parameters and specifications of the RO desalination module.

Parameters	Value (unit)
Effective RO membrane area	0.40 m^2
Water permeability coefficient (A_w)	4.7×10^{-12} $m^3m^{-2}s^{-1}$ Pa^{-1}
Salt permeability coefficient (B_s)	6.9×10^{-8} ms^{-1}
Dimension of the fiberglass pressure vessel	8.38 cm outer diameter and 44.45 cm length
Accumulator volume	473 mL
Accumulator max flow rate	151.42 L min^{-1}
Accumulator pre-charged pressure	3 bars
Saline water concentration	3.50 g/L (1:10 scaled)

4. Experimental results and analysis

4.1. Experimental results and validation

Previous analysis showed an optimal water recovery to achieve the minimal specific energy consumption (*SEC*), defined as the energy required to produce a specific volume of product freshwater with the unit of kWh m^{-3} [38]. Numerical analysis of a direct-drive ocean wave powered SWRO desalination showed that the optimal water recovery for RO is about 25 %. Furthermore, maintaining this water recovery ratio could eliminate the need for chemical pre-treatment [19,13]. As such, we pre-selected this water recovery ratio of 25 % as the baseline water recovery. Based on this ratio, the following procedure for the tank test was adopted. First, for a certain wave height (baseline) in each wave period, we adjusted the needle valve on the brine outlet to ensure a water recovery of about 25 %. Second, with the adjusted needle valve, we considered the pre-selected wave height, i.e., the baseline wave height in Step-1, as the central wave height and tested performance under different wave heights. Finally, upon completing testing under one wave period with different wave heights, we adjusted the needle valve again and repeated the above tests for other wave periods. Because wave power flux is proportional to the wave period and wave height, the baseline wave height was set to 9 cm, 8 cm and 7 cm for 4 s, 4.25 s and 5 s, respectively, based on the capacity of the wavemaker in the wave tank.

The data acquisition system switched off at the start of each test case and switched on once the system was deemed to be stabilized based on the observation of pressure profile. Due to the capacity of the data acquisition system, each run was recorded over 2 min of stable status. After each test, we measured the salt concentration in the brine and the permeate using a portable conductivity meter (*Hach HQ14D*). In order to evaluate the response repeatability, the three auxiliary tests were performed for each test case [40].

The measured feed flux and pressure and the brine concentration under different wave conditions are presented in Fig. 5. The plots show that the feed flux and pressure increased with the wave period and wave height (Fig. 5 A & B). The minimum and maximum feed fluxes obtained in the tank tests were 16.65 $Lm^{-2}h^{-1}$ at $H_s = 7cm\&T_s = 4s$ and 42.75 $Lm^{-2}h^{-1}$ at $H_s = 9cm\&T_s = 5s$, respectively. The minimum and maximum feed pressures obtained in the experiment were 4.68 bars at $H_s = 7cm\&T_s = 4s$ and 9.10 bars at $H_s = 12cm\&T_s = 4s$, respectively. Additionally, brine concentration increased with the wave height at each wave period (Fig. 5C). Meanwhile, the brine concentration depended on the wave period at a specified wave height. The minimum and maximum brine concentrations obtained from the experiment were 4.63 gL^{-1} at $H_s = 7cm/T_s = 4s$ and 7.17 gL^{-1} at $H_s = 12cm\&T_s = 4s$, respectively.

To validate the experimental results with theoretical results, we compare experimental data with the theoretical calculation of the permeate flux (Equation (5) in Section 2) and permeate concentration (Equation (6) in Section 2), as shown in Fig. 6. In the calculations, the water permeability coefficient A_w and salt permeability coefficient B_s were assumed equal to 4.7×10^{-12} $m^3m^{-2}s^{-1}$ $Pa^{-1}$and 6.9×10^{-8} ms^{-1}, respectively. The theoretical values are in good agreement with the experimental measurement in most cases. The minimum and maximum

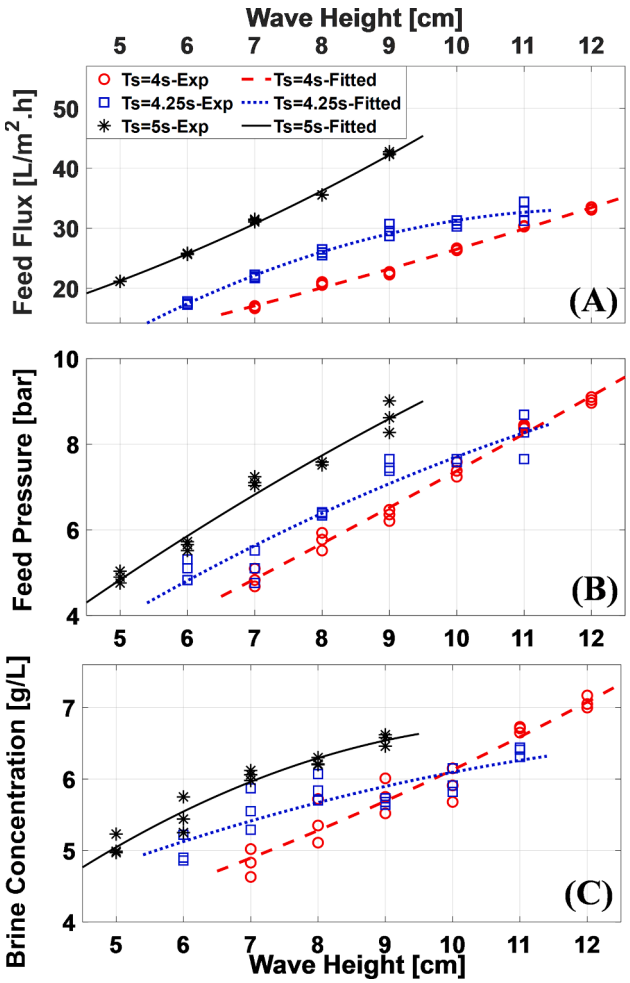

Fig. 5. Experiment results with fitted models at different wave conditions (A) Feed flux. (B) Feed pressure. (C) Brine concentration.

permeate fluxes obtained from the experiment were 2.54 $Lm^{-2}h^{-1}$ at $H_s = 6cm\&T_s = 4.25s$ and 11.81 $Lm^{-2}h^{-1}$ at $H_s = 12cm\&T_s = 4s$, respectively. The maximum and minimum permeate concentration obtained from the experiments were 0.18 gL^{-1} at $H_s = 9cm\&T_s = 4s$ and 0.08 gL^{-1} at $H_s = 10cm\&T_s = 4.25s$, respectively.

With the measured feed and permeate flux, water recovery and salt rejection are calculated accordingly and plotted in Fig. 7. The water recoveries were around 25 % for the baseline wave heights (9 cm for 4 s, 8 cm for 4.25 s and 7 cm for 5 s) and increased with the wave height. Meanwhile, the minimum salt rejection was around 94.71 % at $H_s = 9\,cm\ \&\ T_s = 4s$, and the maximum salt rejection was around 97.74 % at $H_s = 10\,cm\ \&\ T_s = 4.25s$.

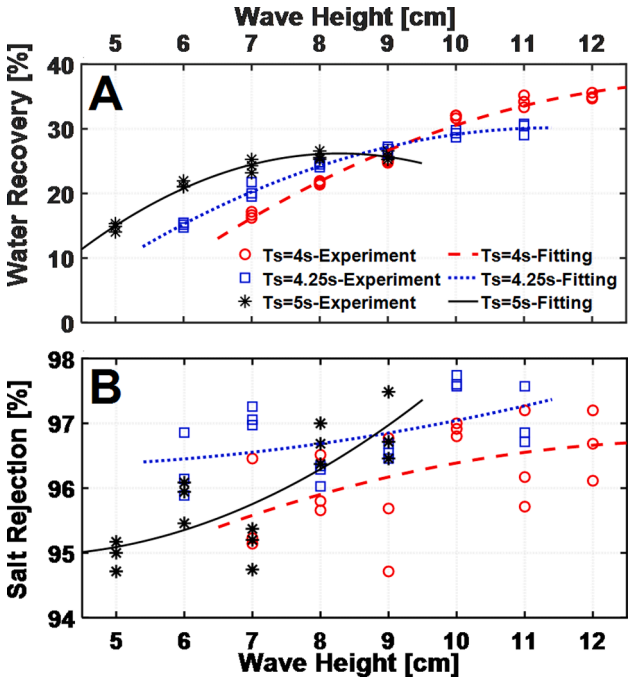

Fig. 7. Experiment results with fitted models at different sea states (A) Water recovery. (B) Salt rejection.

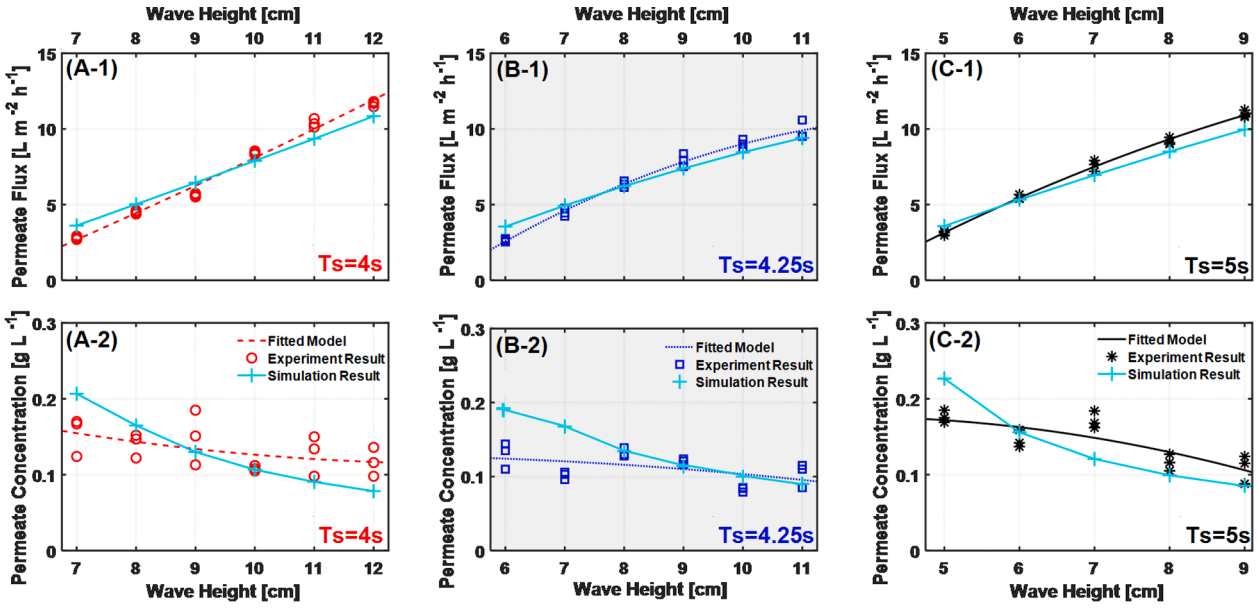

Fig. 6. Permeate flux and permeate concentration at different test conditions.

4.2. Specific water productivity

The specific energy consumption (*SEC*), i.e., the energy consumption to produce a unit volume of freshwater in the unit of kWh per m^3, is one of the crucial metrics used to assess the performance of the desalination process or system [20]. The inverse of *SEC*, defined as the specific water productivity (*SWP*) with a unit of m^3 per kWh (volume of freshwater produced under a unit energy input), can also be used as a metric to evaluate the system performance [41]. For sustainable energy powered desalination system, especially solar-powered desalination, researchers tend to use *SWP* to evaluate the system performance since this metric represents how efficiently the energy captured from sustainable energy resource is used to desalinate water [42,43]. To analyze the energy-water nexus for this sustainable system, we use SWP in this study to evaluate the desalination economy with the captured ocean wave energy.

The maximum *SWP* obtained was 2.23 $m^3 kWh^{-1}$ at $H_s = 10cm$ & $T_s = 4s$ and the minimum *SWP* was 1.41 $m^3\ kWh^{-1}$ at $H_s = 6cm$ & $T_s = 4.25s$, as noted from the plots presented in Fig. 8A. Meanwhile, the *SWP* increased first and then decreased as the wave height increased. The increase in the wave height (i.e., input energy) could adversely affect the economic benefit of desalination beyond a specific wave height. The relationship between the *SWP* and water recovery is shown in Fig. 8B. There is an optimum water recovery for each wave period, as can be observed in Fig. 8B, which may explain the trend in Fig. 8A. Once the needle valve is settled, the water recovery will increase as the wave height increase for a certain wave period. That means the *SWP* will reach to a peak value at the optimal water recovery and decrease once the water recovery is off the optimal value. Furthermore, a larger wave period yielded a smaller optimum water recovery as well as optimum *SWP*. The optimal *SWPs* plotted in Fig. 8B for wave periods 4 s, 4.25 s, and 5 s were 2.10 $m^3\ kWh^{-1}$, 1.97 $m^3\ kWh^{-1}$ and 1.83 $m^3\ kWh^{-1}$ with the corresponding optimal water recovery of 30 %, 25 %, and 21 %, respectively. A summary of the average experiment results is shown in Table 4.

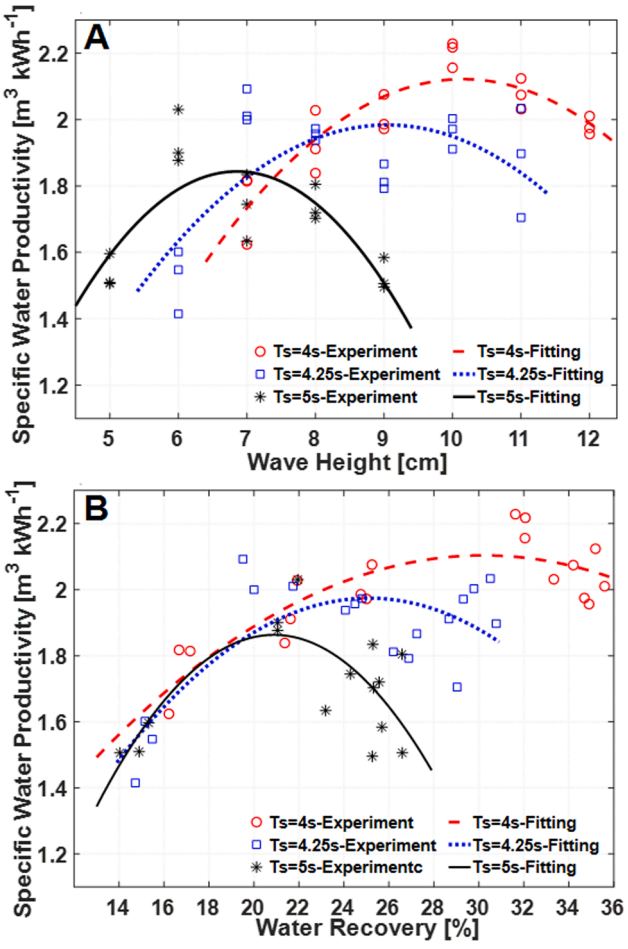

Fig. 8. Specific water productivity analysis of the 1:10 scaled tests. (A) Specific water productivity versus wave height (B) Specific water productivity versus water recovery.

4.3. Effects of key component tuning

As observed in Fig. 8, the *SWP* decreased significantly outside the range of optimal water recovery. Moreover, the system pressure increased as the wave height increased (Fig. 5A), which might exceed the desired pressure range of the RO desalination module and the piston pump at the full scale. To solve these issues, a needle valve on the brine outlet was adopted to adjust the system pressure and water recovery. Beside technical benefits, needle valve tuning for maintaining an optimal water recovery range may also enhance the economics and cost effectiveness of ocean wave powered desalination, as discussed in [20]. Similar operation issues were found in the system-level techno-economic analysis of an autonomous wave-driven desalination system, and there was an optimum load factor in achieving the lowest LCOW [23]. Thus, the needle valve should be tuned appropriately to avoid extreme system pressure under large wave heights while maintaining a good SWP, which will be discussed in this section.

The pre-selected baseline water recovery was 25 % and reached to around 35 % when the wave height reached $H_s = 11cm$ for wave period $T_s = 4.5s$ and $H_s = 12cm$ for wave period $T_s = 4s$, as shown in Fig. 9B-1. Therefore, we tuned the needle valve to increase the brine flowrate and reduce the system pressure by adjusting the needle valve at these points (i.e. $H_s = 11cmat T_s = 4.5s$ and $H_s = 12cmat T_s = 4s$), as shown in Fig. 9 A-2. The average feed pressure dropped at the same wave condition when the needle valve was tuned, as shown in Fig. 9 A-2. The feed pressure reached to 11.80 bars at $T_s = 4.5s$ & $H_s = 11cm$, and decreased by 24 % once the valve was tuned. Since the feed pressure dropped, the reaction force on the piston decreased as defined in Equation (2). Therefore, feed flux slightly increased once the needle valve was tuned at the same wave condition, as shown in Fig. 9A-1. With decreased feed pressure and increased feed flux, the brine concentration decreased (Fig. 9 B-2) while the permeate concentration slightly increased (Fig. 9 C-2).

A plot of the *SWP* versus wave height before and after valve tuning is presented in Fig. 10. For the wave period $T_s = 4.5s$, the *SWP* decreased when the needle valve was tuned. Based on the prediction of the fitted model, tuning the needle valve improved the *SWP* by about 17 % in comparison with its value without tuning (from 1.34 $m^3\ kWh^{-1}$ to 1.57 $m^3\ kWh^{-1}$) at wave height of $H_s = 12\,cm$. However, the *SWP* decreased after valve tuning at wave height $H_s = 12\,cm$ for wave period $T_s = 4s$. Based on the prediction of the fitted model, tuning the needle valve may improve *SWP* if wave height H_s is larger than 14 cm for wave period $T_s = 4s$. That means different wave periods may have different optimum valve tuning parameters.

A plot of the *SWP* versus water recovery before and after needle valve tuning is presented in Fig. 11. The optimal water recovery was around 32 % for the wave period $T_s = 4s$ (Fig. 11A), while around 25 % for the wave period $T_s = 4.5s$ (Fig. 11B). Since the needle valve was tuned once the water recovery reached around 35 %, the valve tuning improved *SWP* for the wave period $T_s = 4.5s$ while underperforming for wave period $T_s = 4s$. Based on these two valve tuning cases, the needle valve should be tuned appropriately for each wave period to keep the system pressure within the desired range to achieve improved performance and good desalination economy. It should be noted that the effect of needle valve tuning is limited, especially under extreme wave conditions. Thus, a pressure-relief valve can be adopted to keep the system pressure within the desired pressure range and a proportion of the captured wave energy

Table 4
Summary of the average experiment results.

Wave Period (s)	Wave Height (cm)	Feed Pressure (bar)	Feed Flux ($Lm^{-2}h^{-1}$)	Permeate Flux ($Lm^{-2}h^{-1}$)	Permeate Concentration (gL^{-1})	Water Recovery (%)	Salt Rejection (%)	*SWP* (m^3 kWh^{-1})
4	7	4.83	17.07	2.81	0.15	16.46	95.71	1.72
	8	5.77	21.04	4.39	0.14	20.87	96.00	1.92
	9	6.36	22.28	5.63	0.15	25.27	95.71	1.99
	10	7.38	26.49	8.54	0.11	32.23	96.86	2.18
	11	8.45	29.90	10.35	0.13	34.61	96.29	2.07
	12	9.03	33.44	11.71	0.12	35.02	96.57	1.97
4.25	6	5.10	17.42	2.75	0.12	15.79	96.57	1.52
	7	5.48	22.15	4.24	0.10	19.14	97.14	2.04
	8	6.39	26.04	6.23	0.13	23.92	96.29	1.96
	9	7.45	29.54	7.94	0.12	26.88	96.57	1.83
	10	7.58	30.71	9.03	0.08	29.40	97.71	1.96
	11	8.21	33.66	9.91	0.10	29.44	97.14	1.88
5	5	4.83	21.22	3.15	0.18	14.84	94.86	1.52
	6	5.65	25.74	5.33	0.16	20.71	95.43	1.92
	7	7.10	31.50	7.65	0.17	24.29	95.14	1.74
	8	7.52	35.55	9.44	0.12	26.55	96.57	1.72
	9	8.62	42.22	10.89	0.11	25.79	96.86	1.52

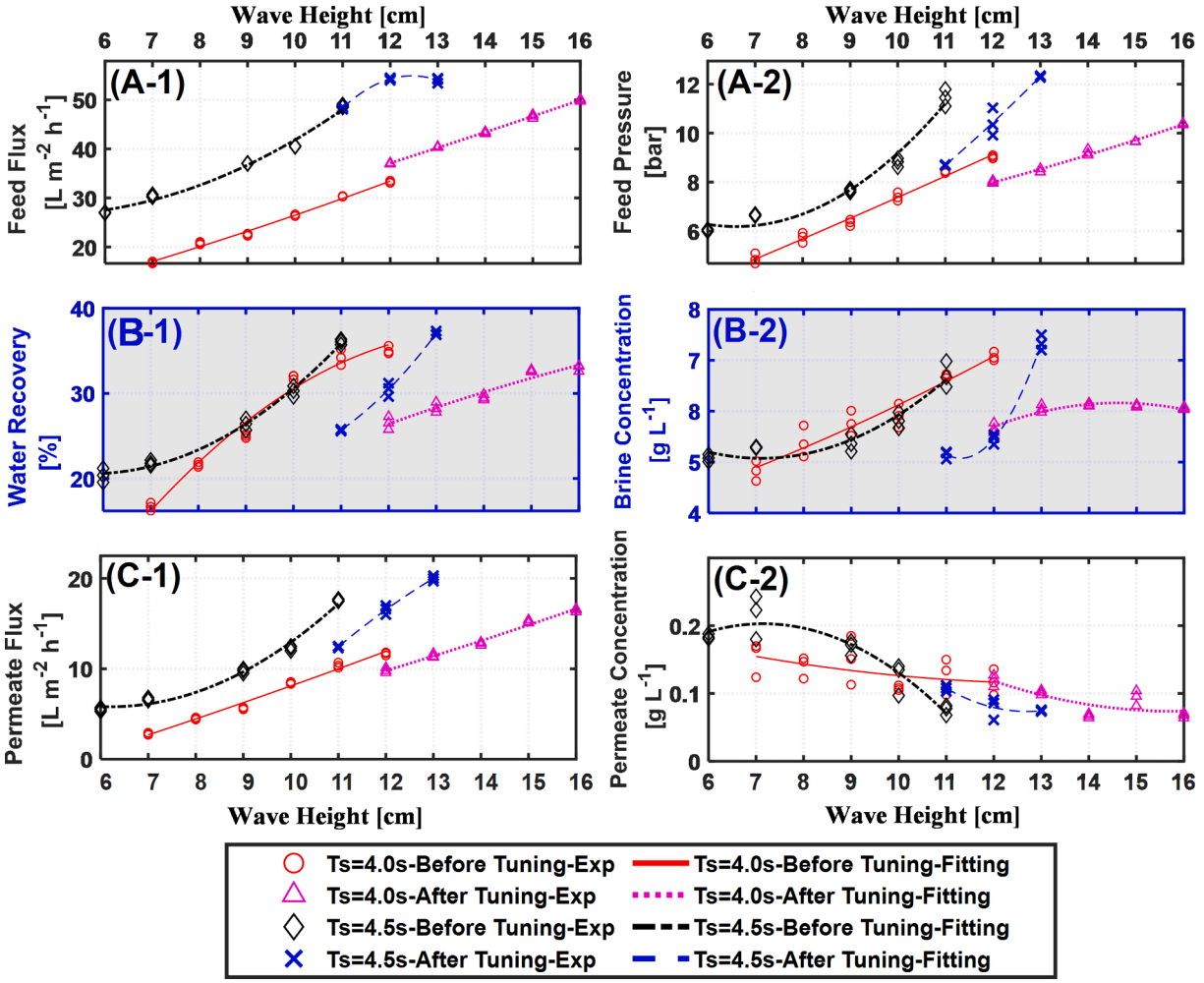

Fig. 9. Experiment results of needle valve tuning. The needle valve is turned at $H_s = 11cm$ for $T_s = 4.5s$ while at $H_s = 12cm$ for $T_s = 4s$ (A-1) Average feed flux; (A-2) Average feed pressure; (B-1) Water Recovery; (B-2). Average brine concentration; (C-1) Average permeate flux; (C-2) Average permeate concentration.

is discarded under large wave conditions due to the limitations of the key components [13,24].

4.4. Comparison and discussion

The practical *SWP* of traditional on-ground RO desalination plant (the yellow region in Fig. 12) is around 0.17–0.32 m^3 kWh^{-1} based on the database [5,44]. The reported practical RO desalination units powered by solar photovoltaic (PV) is around 0.13–0.26 m^3 kWh^{-1} (the shade region in Fig. 12) based on the summary between 2007 and 2017 [45]. Simulation results of a single ocean wave powered RO system (green region in Fig. 12) indicated around 0.24–0.31 m^3 kWh^{-1} *SWP*

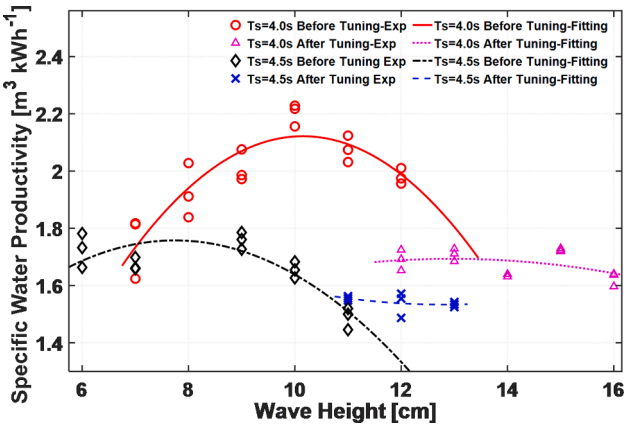

Fig. 10. Specific water productivity versus wave height before and after needle valve tuning.

under different sea states. This means a wave powered RO desalination system is competitive compared to on-ground RO desalination plant powered by fossil fuel [20]. In addition, simulation results of a large wave farm with a 100-device array (blue dotted line) indicated a promising *SWP* of 0.36 m^3 kWh^{-1}, which is better than the on-ground RO desalination plant powered by fossil fuel. The performance of an ocean wave powered desalination system was experimentally investigated in a 1:10 scaled model in this study. To estimate the prototype performance and compare with other scenarios, the experimental results of the scaled tank test in Section 4.2 were converted to full scale based on the Froude scaling law (as shown in Table 1) [33]. The prediction after conversion based on this 1:10 scaled pilot experimental results under different sea states is noted as a red line in Fig. 12. The fitted red line in Fig. 12 set in the lower part of the on-ground RO desalination plant performance (yellow region). That means this pilot study revealed experimentally that the proposed ocean wave powered desalination is promising compared with traditional technologies using fossil fuel and solar PV. This pilot study reveals the similar findings that ocean wave powered RO is promising for large scale scenarios considering the energy consumption and the LCOW, as stated in [45]. However, ocean wave powered RO is still mainly in the basic research level but PV-powered RO has already been adopted in the application level [45]. It should be noted that, experimental prediction based on this study is related to water recovery, but the relationship between *SWP* and water recovery are unknown for other scenarios (simulation and practical) from literature. Therefore, only the experiment prediction in this study is shown with the relationship to water recovery (red line in Fig. 12) while all the other cases just represent their reported *SWP* and not related to water recovery.

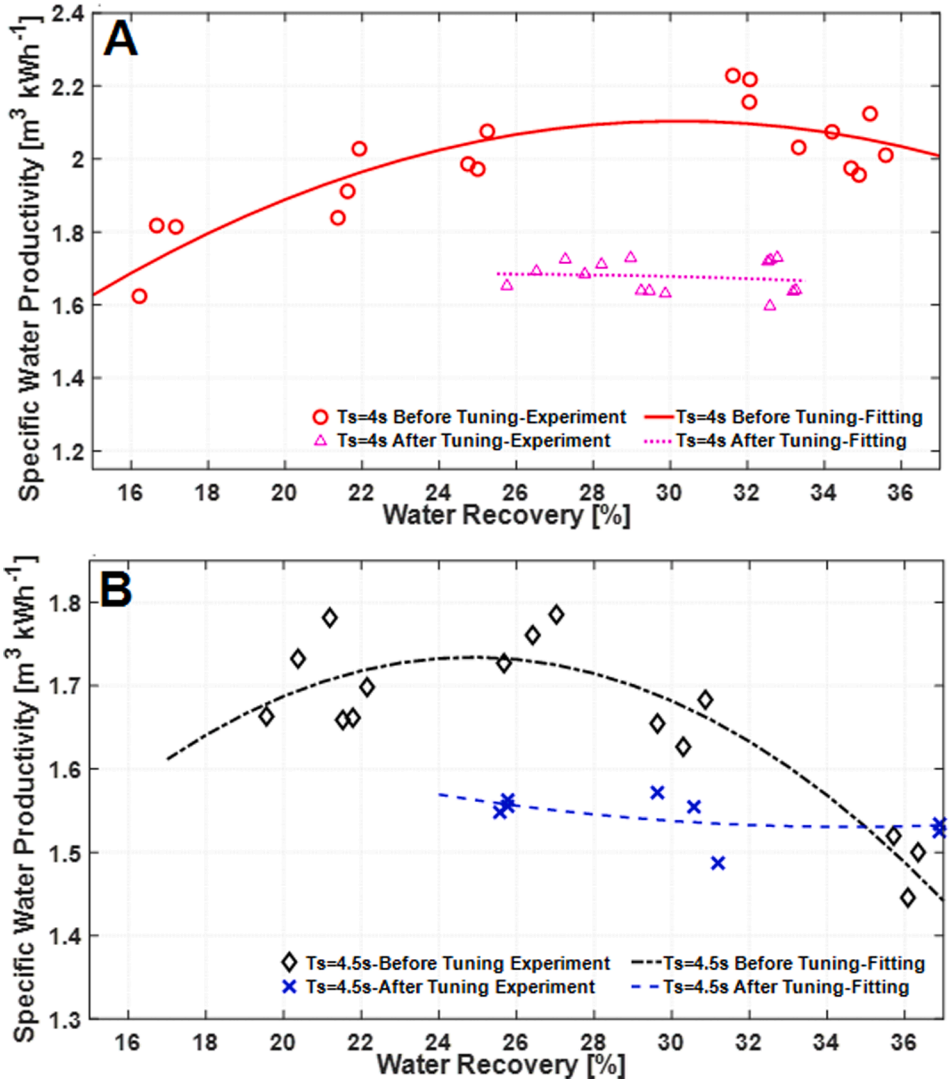

Fig. 11. Specific water productivity versus water recovery before and after valve tuning (A) Wave period $T_s = 4s$ (B) Wave period $T_s = 4.5s$.

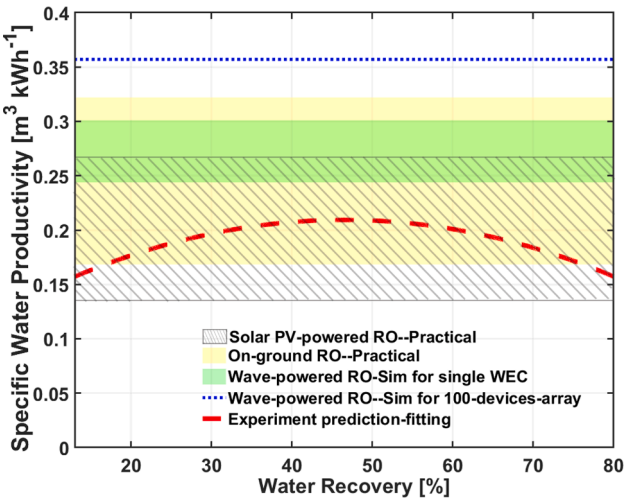

Fig. 12. Comparison of the full-scale practical specific water productivity. Solar PV-powered RO is based on the survey between 2007 and 2017 in [45]. On-ground RO is based on the practical database [5,44]. The simulation results of a single WEC ocean wave powered RO are based on different wave conditions [20]. The simulation result of a 100-device array is based on the utility-scale modeling in the U.S [24]. Experiment prediction is based on the 1:10 scaled pilot experiment results in Section 4.2 and converted to full-scale in real application based on the Froude Scaling Law [33].

In the future, energy saving technologies, such as energy recovery devices (ERDs) and batch-mode operation [20,46], could be implemented into the proposed system to enhance the system's performance further. Meanwhile, techno-economic analysis should be performed to investigate the economic benefits of the proposed system [23,24]. Additionally, system level optimization and critical components sizing, such as the accumulator and needle valve, are worth further investigations to improve the system performance. It should be noted that system level optimization under time-varying wave conditions is very complicated, which requires powerful methods. In solar-powered desalination system, approaches using machine learning have been discussed and found it can effectively improve the system performance [47,48]. Similar approaches using machine learning or other powerful methods are worth to be investigated in the future.

5. Conclusions

We experimentally investigated and analyzed a wave powered reverse osmosis (RO) desalination system via scaled system demonstration in a wave tank. A double-acting piston pump was driven by an oscillating surge wave energy converter (OSWEC) and used to directly pressurize saline water. A bladder-type accumulator was used to mitigate the pressure fluctuations under time-varying wave conditions. To keep the system pressure within the desired range and maintain a good operation economy, the brine outlet was regulated by a needle valve. Because of the wave tank capacity, the physical model was scaled down by 10 times based on the Froude scaling law with the flap length of 1.8 m and feed salinity of 3.5 g L^{-1}. Experimental results revealed that the maximum permeate flux and salt rejection obtained were 11.81 $Lm^{-2}h^{-1}$ and 97.74 %, respectively. To evaluate the energy consumption effectiveness, specific water productivity (*SWP*) with the unit of m^3 per kWh of input power was introduced. The needle valve on the brine outlet was tuned to evaluate the influence on system pressure and *SWP*. The maximum *SWP* of the scaled system demonstration was 2.23 m^3 kWh^{-1} with the corresponding optimum water recovery of 32 % and the *SWP* descended once the water recovery was off the optimal water recovery. In a specific case, tuning of the needle valve resulted in 17 % improvement of *SWP* and 24 % reduction of the system pressure, pointing to the possibility of avoiding abnormal system pressure under extreme wave conditions while maintaining a good energy consumption effectiveness. Prediction of the full-scale scenarios from this pilot study indicated that this integrated wave powered RO desalination is promising compared to the on-ground RO desalination plant powered by fossil fuel and solar PV, and system optimization as well as energy recovery technologies are worth further investigating to improve the system's performance.

CRediT authorship contribution statement

Jia Mi: Conceptualization, Methodology, Investigation, Validation, Writing – original draft, Visualization. **Xian Wu:** Formal analysis, Investigation, Writing – review & editing. **Joseph Capper:** Conceptualization, Writing – review & editing. **Xiaofan Li:** Data curation, Formal analysis. **Ahmed Shalaby:** Investigation, Writing – review & editing. **Ruoyu Wang:** Methodology, Formal analysis. **Shihong Lin:** Conceptualization, Methodology, Writing – review & editing. **Muhammad Hajj:** Conceptualization, Supervision, Project administration, Funding acquisition, Writing – review & editing. **Lei Zuo:** Conceptualization, Supervision, Project administration, Funding acquisition, Writing – review & editing.

Declaration of Competing Interest

The authors declare that they have no known competing financial interests or personal relationships that could have appeared to influence the work reported in this paper.

Data availability

Data will be made available on request.

Acknowledgement

The authors would like to thank the support from the U.S. National Science Foundation (CBET-1903627) and the U.S. Agency for International Development (USAID) as well as the National Academy Sciences (NAS) through Sub award #2000009131. The authors would like to thank the raw materials and components partially shared from another project funded by the U.S. Department of Energy (DE-EE0008953). The authors would like to thank the support from the *"Waves to Water Prize"* launched by the U.S. National Renewable Energy Laboratory. In addition, the authors would like to acknowledge the support from research assistants and technicians from the Davidson Laboratory at Stevens Institute of Technology, especially for Mr. Raju Datla, Mr. Uihoon Chuang and Ms. Alaa Ahmed on prototype preparation and setup. The authors would like to thank Erin Jones for the proof reading and Qiaofeng Li for valuable discussion.

References

[1] Naddeo V. One planet, one health, one future: the environmental perspective. Water Environ Res 2021;93:1472–5. https://doi.org/10.1002/wer.1624.
[2] Cavagnaro RJ, Copping AE, Green R, Greene D, Jenne S, Rose D, et al. Powering the blue economy: progress exploring marine renewable energy integration with ocean observations. Mar Technol Soc J 2020;54:114–25. https://doi.org/10.4031/MTSJ.54.6.11.
[3] Gain AK, Giupponi C, Wada Y. Measuring global water security towards sustainable development goals. Environ Res Lett 2016:11. https://doi.org/10.1088/1748-9326/11/12/124015.
[4] Hanak E, Mount J, Chappelle C, Lund J, Medellín-Azuara J, Moyle P, et al. What if California's drought continues? Vol. 29. San Francisco; 2015.
[5] Lin S, Veerapaneni S. Emerging investigator series: toward the ultimate limit of seawater desalination with mesopelagic open reverse osmosis. Environ Sci Water Res Technol 2021;7:1212–9. https://doi.org/10.1039/d1ew00153a.
[6] Slocum AH, Haji MN, Trimble AZ, Ferrara M, Ghaemsaidi SJ. Integrated pumped hydro reverse osmosis systems. Sustain Energy Technol Assess 2016;18:80–99. https://doi.org/10.1016/j.seta.2016.09.003.
[7] Xie J, Zuo L. Dynamics and control of ocean wave energy converters. Int J Dyn Control 2013;1:262–76. https://doi.org/10.1007/s40435-013-0025-x.

[8] Kilcher L, Fogarty M, Lawson M. Marine energy in the United States: an overview of opportunities; 2021. doi: 10.2172/1766861.

[9] Davies PA. Wave-powered desalination: resource assessment and review of technology. Desalination 2005;186:97–109. https://doi.org/10.1016/J.DESAL.2005.03.093.

[10] Sharmila N, Jalihal P, Swamy AK, Ravindran M. Wave powered desalination system. Energy 2004;29:1659–72. https://doi.org/10.1016/J.ENERGY.2004.03.099.

[11] Hicks DC, Mitcheson GR, Pleass CM, Salevan JF. Delbouy: ocean wave-powered seawater reverse osmosis desalination systems. Desalination 1989;73:81–94. https://doi.org/10.1016/0011-9164(89)87006-7.

[12] Whittaker T, Folley M. Nearshore oscillating wave surge converters and the development of Oyster. Philos Trans R Soc A: Math Phys Eng Sci Vol. 370. Royal Society; 2012. p. 345–64. doi: 10.1098/rsta.2011.0152.

[13] Folley M, Peñate Suarez B, Whittaker T. An autonomous wave-powered desalination system. Desalination 2008;220:412–21. https://doi.org/10.1016/J.DESAL.2007.01.044.

[14] Ylänen MMM, Lampinen MJ. Determining optimal operating pressure for AaltoRO – a novel wave powered desalination system. Renew Energy 2014;69:386–92. https://doi.org/10.1016/J.RENENE.2014.03.061.

[15] Keshavarz P, Zolghadr M, Mohammad S, Zomorodian A. Seawater transfer to onshore using a paddle type wave energy converter. J Mar Eng 2021;17(34):99.

[16] Li Q, Mi J, Li X, Chen S, Jiang B, Zuo L. A self-floating oscillating surge wave energy converter. Energy 2021;230:120668. https://doi.org/10.1016/j.energy.2021.120668.

[17] Capper J, Mi J, Li Q, Zuo L. Numerical analysis and parameter optimization of a portable two-body attenuator wave energy converter. In: ASME 2021 Int. Des. Eng. Tech. Conf. Comput. Inf. Eng. Conf., 2021. doi: 10.1115/DETC2021-69977.

[18] Cheddie D, Maharajh A, Ramkhalawan A, Persad P. Transient modeling of wave powered reverse osmosis. Desalination 2010;260:153–60. https://doi.org/10.1016/J.DESAL.2010.04.048.

[19] Yu YH, Jenne D. Numerical modeling and dynamic analysis of a wave-powered reverse-osmosis system. J Mar Sci Eng 2018:6. https://doi.org/10.3390/jmse6040132.

[20] Brodersen KM, Bywater EA, Lanter AM, Schennum HH, Furia KN, Sheth MK, et al. Direct-drive ocean wave-powered batch reverse osmosis. Desalination 2022;523:115393. https://doi.org/10.1016/J.DESAL.2021.115393.

[21] Cabrera P, Folley M, Carta JA. Design and performance simulation comparison of a wave energy-powered and wind-powered modular desalination system. Desalination 2021;514:115173. https://doi.org/10.1016/J.DESAL.2021.115173.

[22] Zhou Q, Guo S, Xu L, Guo X, Williams H, Xu H, et al. Global optimization of the hydraulic-electromagnetic energy-harvesting shock absorber for road vehicles with human-knowledge-integrated particle swarm optimization scheme. IEEE/ASME Trans Mechatron 2021;26:1225–35. https://doi.org/10.1109/TMECH.2021.3055815.

[23] Folley M, Whittaker T. The cost of water from an autonomous wave-powered desalination plant. Renew Energy 2009;34:75–81. https://doi.org/10.1016/J.RENENE.2008.03.009.

[24] Yu Y-H, Jenne D. Analysis of a wave-powered, reverse-osmosis system and its economic availability in the United States. In: ASME 2017 36th Int. Conf. Ocean. Offshore Arct. Eng.; 2017. doi: 10.1115/OMAE2017-62136.

[25] Portillo JCC, Collins KM, Gomes RPF, Henriques JCC, Gato LMC, Howey BD, et al. Wave energy converter physical model design and testing: The case of floating oscillating-water-columns. Appl Energy 2020;278:115638. https://doi.org/10.1016/J.APENERGY.2020.115638.

[26] Gomes RPF, Gato LMC, Henriques JCC, Portillo JCC, Howey BD, Collins KM, et al. Compact floating wave energy converters arrays: Mooring loads and survivability through scale physical modelling. Appl Energy 2020;280:115982. https://doi.org/10.1016/J.APENERGY.2020.115982.

[27] Li X, Chen CA, Li Q, Xu L, Liang C, Ngo K, et al. A compact mechanical power take-off for wave energy converters: design, analysis, and test verification. Appl Energy 2020;278:115459. https://doi.org/10.1016/J.APENERGY.2020.115459.

[28] Ruehl K, Forbush DD, Yu YH, Tom N. Experimental and numerical comparisons of a dual-flap floating oscillating surge wave energy converter in regular waves. Ocean Eng 2020;196:106575. https://doi.org/10.1016/J.OCEANENG.2019.106575.

[29] Elhanafi A, Macfarlane G, Fleming A, Leong Z. Experimental and numerical investigations on the hydrodynamic performance of a floating–moored oscillating water column wave energy converter. Appl Energy 2017;205:369–90. https://doi.org/10.1016/J.APENERGY.2017.07.138.

[30] Elhanafi A, Macfarlane G, Fleming A, Leong Z. Scaling and air compressibility effects on a three-dimensional offshore stationary OWC wave energy converter. Appl Energy 2017;189:1–20. https://doi.org/10.1016/J.APENERGY.2016.11.095.

[31] Leijon J, Salar D, Engström J, Leijon M, Boström C. Variable renewable energy sources for powering reverse osmosis desalination, with a case study of wave powered desalination for Kilifi, Kenya. Desalination 2020;494:114669. https://doi.org/10.1016/j.desal.2020.114669.

[32] Abdelkareem MAA, Xu L, Ali MKA, Elagouz A, Mi J, Guo S, et al. Vibration energy harvesting in automotive suspension system: a detailed review. Appl Energy 2018;229:672–99. https://doi.org/10.1016/j.apenergy.2018.08.030.

[33] LiVecchi A, Copping A, Jenne D, Gorton A, Preus R,Gill G, et al. Powering the blue economy: exploring opportunities for marine renewable energy in maritime markets. Washington, D.C.; 2019.

[34] McWhorter J, Wright D, Thomas J. Coastal data information program (CDIP). Res Ideas Outcomes 2016;2:e8827.

[35] Dallman AR, Neary VS. Characterization of U.S. Wave Energy Converter (WEC) test sites: a catalogue of met-ocean data. Sandia Natl Lab; 2015. p. 304.

[36] Millero FJ, Feistel R, Wright DG, McDougall TJ. The composition of Standard Seawater and the definition of the Reference-Composition Salinity Scale. Deep Sea Res Part I Oceanogr Res Pap 2008;55:50–72. https://doi.org/10.1016/J.DSR.2007.10.001.

[37] Mi J, Wu X, Capper J, Li X, Shalaby A, Chung U, et al. Modelling, characterization and testing of an ocean wave powered desalination system. Proc ASME Des Eng Tech Conf 2022;10:1–8. https://doi.org/10.1115/DETC2022-91285.

[38] Membranes and modules. Membr Technol Appl. John Wiley & Sons, Ltd; 2012. p. 97–178. doi: 10.1002/9781118359686.ch3.

[39] Sarai Atab M, Smallbone AJ, Roskilly AP. An operational and economic study of a reverse osmosis desalination system for potable water and land irrigation. Desalination 2016;397:174–84. https://doi.org/10.1016/J.DESAL.2016.06.020.

[40] Wei QJ, Tucker CI, Wu PJ, Trueworthy AM, Tow EW, Lienhard JH. Impact of salt retention on true batch reverse osmosis energy consumption: experiments and model validation. Desalination 2020;479:114177. https://doi.org/10.1016/J.DESAL.2019.114177.

[41] Wang L, Zhang C, He C, Waite TD, Lin S. Equivalent film-electrode model for flow-electrode capacitive deionization: experimental validation and performance analysis. Water Res 2020;181:115917. https://doi.org/10.1016/J.WATRES.2020.115917.

[42] Wang Z, Horseman T, Straub AP, Yip NY, Li D, Elimelech M, et al. Pathways and challenges for efficient solar-thermal desalination. Sci Adv 2019;5. https://doi.org/10.1126/sciadv.aax0763.

[43] Xue G, Chen Q, Lin S, Duan J, Yang P, Liu K, et al. Highly efficient water harvesting with optimized solar thermal membrane distillation device. Glob Challenges 2018;2:1800001. https://doi.org/10.1002/gch2.201800001.

[44] LiVecchi A, Copping A, Jenne D, Gorton A, Preus R, Gill G, et al. Powering the blue economy: exploring opportunities for marine renewable energy in maritime markets. Washington, D.C.; 2019.

[45] Abdelkareem MA, El Haj AM, Sayed ET, Soudan B. Recent progress in the use of renewable energy sources to power water desalination plants. Desalination 2018;435:97–113. https://doi.org/10.1016/J.DESAL.2017.11.018.

[46] Werber JR, Deshmukh A, Elimelech M. Can batch or semi-batch processes save energy in reverse-osmosis desalination? Desalination 2017;402:109–22. https://doi.org/10.1016/J.DESAL.2016.09.028.

[47] Pombo DV, Bindner HW, Spataru SV, Sørensen PE, Rygaard M. Machine learning-driven energy management of a hybrid nuclear-wind-solar-desalination plant. Desalination 2022;537. https://doi.org/10.1016/j.desal.2022.115871.

[48] Kandeal AW, An M, Chen X, Algazzar AM, Kumar Thakur A, Guan X, et al. Productivity modeling enhancement of a solar desalination unit with nanofluids using machine learning algorithms integrated with Bayesian optimization. Energy Technol 2021;9:1–11. https://doi.org/10.1002/ente.202100189.